Int J Mech Mater Des (2016) 12:193–209
DOI 10.1007/s10999-015-9301-6

Influence of surface energy on the nanoindentation response of elastically-layered viscoelastic materials

Alaa A. Abdel Rahman · Ahmed G. El-Shafei · Fatin F. Mahmoud

Received: 13 October 2014 / Accepted: 2 March 2015 / Published online: 10 March 2015

Abstract In the context of integrated nonlinear viscoelastic contact mechanics, a nonlinear finite element model is developed to predict and analyze the quasistatic response of nanoindentation problems of an elastically-layered viscoelastic materials considering the surface elasticity effects. Effects of surface energy are accounted for by employing the Gurtin–Murdoch continuum model for surface elasticity. The linear viscoelastic response is modeled by the Schapery's creep model with a Prony's series to express the transient component in the creep compliance. The viscoelastic constitutive equations are cast into a recursive form that needs only the previous time increment rather than the entire strain history. To satisfy the contact constraints exactly, the Lagrange multiplier method is adopted to enforce the contact conditions into the system. The equilibrium indentation configuration is obtained through the Newton–Raphson iterative procedure. The developed model is verified then applied to investigate the quasistatic nanoindentation response of two different indentation problems with different geometry and loading conditions. Results show the significant effects of surface energy and viscoelasticity on the quasistatic nanoindentation response.

Keywords Surface energy · Gurtin–Murdoch continuum model · Schapery's viscoelasticity · Nanoindentation · Finite element method

1 Introduction

Nanoindentations have become one of the most popular mechanical characterization techniques in the last decade. These techniques have been widely used to measure the mechanical properties of different materials; ceramics (Hainsworth and Page 1994), metals (Beegan et al. 2007) and metal ceramic multilayers (Tang et al. 2008). In these techniques, it was demonstrated that when the indenter size decreases to micrometers or nanometers, the indentation response show a significant dependence on the indenter size Nix and Gao 1998; Huang 2008). Mechanical behavior of nanostructured materials can be investigated by two basic approaches; experimental methods and theoretical simulations. The experimental approach basically yields results reflecting the real behaviors but it has been found highly dependent on experimental settings and, generally, expensive. For

A. A. Abdel Rahman (✉) · A. G. El-Shafei · F. F. Mahmoud
Department of Mechanical Design and Production Engineering, College of Engineering, Zagazig University, Zagazig 44511, Egypt
e-mail: alaaabouahmed@gmail.com

A. G. El-Shafei
e-mail: agelshafei@yahoo.com

F. F. Mahmoud
e-mail: faheem@aucegypt.edu

the theoretical approach, though existing molecular simulations offer advantages in precise response prediction, they require simultaneously intensive computational resources associated with the modeling of a large number of degrees of freedom at a nanoscale. Due to such highly demanding requirement, applications of those techniques to modeling practical problems have been quite limited. The continuum based approach is therefore considered as an attractive alternative since the use of simplified governing physics dramatically reduces the computational cost. The classical continuum theory generally neglects the presence of intrinsic size and thus seems incapable of demonstrating the size dependent behavior of nanostructured materials. The size dependency of material behaviors at a nanoscale has been well recognized due to their relatively high surface to volume ratio whereas, in the case of soft elastic materials, the intrinsic length scale, which is defined as the ratio of surface free energy and Young's modulus (Yakobson 2003), is much larger than that of conventional solids and becomes comparable to the characteristic length of the material element in practical situations (He and Lim 2006).

Real surfaces and interfaces may have much more complicated morphologies and microstructures which present as another mechanism of surface effects in addition to the surface residual stresses. Using both molecular dynamics and FE simulations, Wang et al. (2015) investigated the elastic compression of crystalline nanoparticles. It was shown that the atomic-scale surface roughness plays an important role in the elastic deformation of nanoparticles. As the particle radius increases from nanometers to micrometers, the effects of atomic-scale surface steps become negligible. Chen and Diebels (2014) developed a procedure to analyze and to characterize polymers from nanoindentation using the FEM based inverse method. Surface roughness, adhesion force, and the real shape of the tip are involved in the numerical model.

Comprehensive literature review on the surface energy effects and the Gibbsian formulation of the thermodynamics of surfaces can be found in many researches on surface and interface stresses (Cammarata 1994, 1997; Fischer et al. 2008). To study the mechanical behavior of an immediate neighborhood of material surfaces through a continuum-based model (Gurtin and Murdoch 1975, 1978; Gurtin et al. 1998) developed a mathematical framework to account for the influence of surface free energy. In that model, the existing surface is simply represented by thin layer perfectly bonded to the bulk and its behavior is governed by a constitutive law different from that of the bulk. In the study of nanoscale problems, all material constants in the constitutive model were commonly calibrated with data obtained from either experimental measurements (Jing et al. 2006) or atomistic simulations (Miller and Shenoy 2000; Shenoy 2005). Upon various verifications and comparisons with results predicted by atomistic and molecular static simulations (Dingreville et al. 2005), Gurtin–Murdoch surface elasticity model has proven promising and attractive for modeling a variety of nanoscale problems to account for the influence of surface free energy. The model has gained rapid recognition from various researchers and been widely used in the investigation of mechanical responses of nanostructures; ultra-thin elastic films (He et al. 2004; Huang 2008), thin plates (Lu et al. 2006), nanoscale inhomogeneities (Sharma et al. 2003; Duan et al. 2005; Sharma and Wheeler 2007; Tian and Rajapakse 2007), dislocations (Intarit et al. 2010) and nanoscale elastic layers (Intarit et al. 2011; Zhao 2009; Zhao and Rajapakse 2009, 2013). This should additionally confirm the benefit of employing such alternative continuum-based model to save the computational resources with an acceptable level of accuracy gained.

Modeling of nanoindentation problems via the use of suitable mathematical models offered an attractive candidate for investigating various aspects and gaining fundamental insight of material properties. Based on the surface elasticity theory, Huang and Yu (2007) formulated 3D and 2D surface Green's function, respectively. Through the Fourier integral transformation method, Wang and Feng (2007) derived the elastic field induced by a concentrated force acting on a half space with surface tension. Using Stroh's formalism, Koguchi (2008) obtained the surface Green's function of an anisotropic half space with surface effects. Chen and Zhang (2010) presented the corresponding surface Green's function for anti-plane shear deformation. Long et al. (2012) formulated the indention of a 3D contact problem between a sphere and a half space with surface tension. This work was extended by Long and Wang (2013) who considered the axisymmetric contact between a rigid sphere and an elastic half space. Pinyochotiwong et al. (2013) proposed a continuum based concepts in the analysis

of an axisymmetric rigid frictionless indenter acting on an isotropic, linearly elastic half space. The influence of surface stresses is considered by employing a complete Gurtin–Murdoch continuum model for surface elasticity. Using the general form of the linearized surface elasticity theory of Gurtin and Murdoch, Zhou and Gao (2013) derived analytical solutions for the problems of an elastic half space subjected to a distributed normal force. Fourier transforms and Bessel functions were utilized in the formulation.

Numerical solutions for the nanostructured solids are obtained by using the FEM. Gao et al. (2006) developed a FE model to investigate the size dependent mechanical behavior of nanostructures by developing a kind of surface element to take into account the surface elastic effect. Wang et al. (2010) investigated the size dependent deformations of two dimensional nanosized structures with surface effects by the finite element method. Truss element was used to evaluate the contribution of surface stress to the total potential energy. Liu et al. (2011) presented a finite element formulation of a non-classical beam theory based on the Gurtin–Murdoch model for continua with deformable elastic surfaces. Considering functionally graded materials (FGM), Shaat et al. (2013a, b), developed a finite element model to investigate the mechanical behavior of nanostructured FGM considering the surface energy effects. Gad et al. (2014) proposed a finite element model to solve and analyze the nanoindentation problems in elastic solids considering the surface energy effect. The surface energy effect is modeled by Gurtin and Murdoch theory of surface elasticity. The proposed model has been used to study the effects of surface energy, taking into account the second order displacement gradient, on the mechanical behavior of nanostructures under indentation test (Attia et al. 2015).

It is important to mention that most of the cited references in the literature, e.g. (Zhou and Gao 2013; Long et al. 2012; He and Lim 2006), treated the nanoindentation contact problem as a stress analysis problem. Firstly, the analytical contact models such as Hertz model is firstly exploited to determine the contact pressure distribution and the contact length. Those classical models had been developed based on classical elasticity and ignoring of the surface effects. Afterwards, the obtained classical contact pressure is taken as an external applied load to investigate the indentation response as a stress analysis problem, but taking surface effect into account.

The main objective of the present paper is to develop a nonlinear FE model for handling nanoindentation of elastically-layered viscoelastic bodies in the framework of integrated contact mechanics. The model accounts for surface effects by adopting the Gurtin–Murdoch surface elasticity model. This integrated model consists of two consecutive parts; the first one stands as solution of the contact problem between the indenter and the indented continuum, to determine contact pressure distribution and the extension of contact area. The second part exploits the contact results to investigate the indentation response of the continuum subjected to contact pressure distribution. Both parts of the model have taken surface effects into account. The Schapery's single-integral creep model is adopted to model the linear viscoelastic response. The Lagrange multiplier method is used to exactly satisfy contact constraints without any insertion of penalty parameters. The obtained results show remarkable effects of both surface energy and viscoelasticity on the quasistatic nanoindentation response of elastically-layered viscoelastic solids.

2 Formulation of nanoindentation problem with surface energy effect

Consider a 2D frictionless nanoindentation problem of an elastically-layered viscoelastic layer intended by a rigid indenter as shown in Fig. 1. The domain of the problem is decomposed into two major parts; the

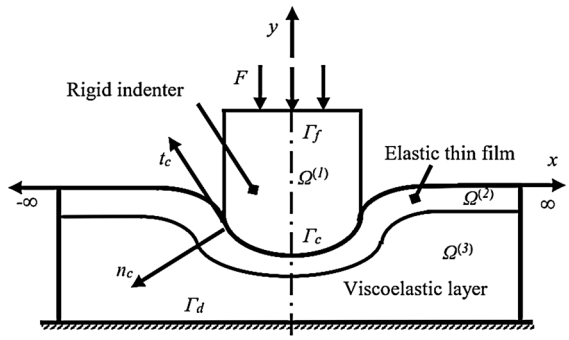

Fig. 1 Schematic representation of an indentation problem

indenter domain $\Omega^{(1)}$ and the indented body which is composed of two parts; the elastic domain of the thin film $\Omega^{(2)}$ and the viscoelastic layer domain $\Omega^{(3)}$. Moreover, the elastic domain, $\Omega^{(2)}$ is decomposed into two parts; the bulk of the elastic coating denoted by $\Omega^{(2)\mathrm{B}}$ and the surface denoted by S. A surface S is defined as a layer of zero thickness located at the top boundary of $\Omega^{(2)}$ and perfectly bonded to it. According to this definition of the surface, the geometry of the bulk $\Omega^{(2)\mathrm{B}} \cup \Omega^{(3)}$ is identical to that of $\Omega^{(2)} \cup \Omega^{(3)}$. The top surface of the elastic film possesses a constant residual surface tension τ_s in the unstrained state and surface Lame's constants μ_s and λ_s. The boundary of the bulk is subjected to the unknown traction t^b exerted directly by the surface S whereas S is treated as a two-sided surface with the top side compressed by the indenter and the bottom side subjected to the traction t^s exerted by the bulk. The boundary is decomposed into three parts Γ_d, Γ_f and Γ_c. Γ_d and Γ_f are the two portions of the boundary on which displacement and normal traction are prescribed, respectively. On the other hand, Γ_c is the portion of the boundary that contains material surfaces which candidate to come into contact upon the application of loads. In addition to the boundary conditions that prescribed on the boundary Γ_d, a set of contact constraints should be imposed throughout the indentation surface Γ_c. The behavior of the bulk $\Omega^{(2)\mathrm{B}} \cup \Omega^{(3)}$ are modeled by a classical theory of linear elasticity and linear viscoelasticity, respectively. Governing equilibrium equations, constitutive equations, boundary conditions and contact constraints are expressed as follows:

In the absence of a body force, and for quasistatic condition, the governing equilibrium equations of the bulk can be expressed as (Gad et al. 2014):

$$ {}^{t}\sigma^{B}_{ij,j} = 0 \quad (\text{in } \Omega, \mathrm{t}) \tag{1} $$

With small deformation and small rotation, the strain–displacement relationship is defined as:

$$ {}^{t}\varepsilon^{B}_{ij} = \frac{1}{2}\left(u^{B}_{i,j} + u^{B}_{j,i}\right) \tag{2} $$

where ${}^{t}\sigma^{B}_{ij}$ and ${}^{t}\varepsilon^{B}_{ij}$ are the bulk stress and strain tensors, respectively.

The kinematic and kinetic boundary conditions can be written as:

$$ u_i = 0 \quad (\text{on } \Gamma_d, t) \quad \text{and} \quad F_i = \sigma_{ij} n_j \quad (\text{on } \Gamma_f, t) \tag{3} $$

Assuming the surface S is adhered perfectly to the bulk $\Omega^{(2)\mathrm{B}}$ without slipping, the displacement and traction along the interface of the surface and the bulk must be continuous. This renders the following continuity conditions:

$$ u^{s}_{i} = u_i\big|_{y=0}, \quad t^{s}_{i} = -t^{B}_{i}, \qquad t^{B}_{i} = -\sigma^{B}_{i2}\big|_{y=0} \tag{4} $$

The initial conditions can be written as:

$$ \left.\begin{array}{ll} u^{B}_{i}(x_k,t) = u^{B}_{oi} & u^{s}_{i}(x_k,t) = u^{s}_{oi} \\ \sigma^{B}_{ij}(x_k,t) = \sigma^{B}_{oij} & \sigma^{s}_{ij}(x_k,t) = \sigma^{s}_{oij} \end{array}\right\} at \quad t = 0 \tag{5} $$

In addition to the boundary conditions (3), (4) and assuming frictionless contact condition, the following contact conditions must be imposed for all contact points at the indentation surface, (Pinyochotiwong et al. 2013):

$$ \left.\begin{array}{l} G_n = u_n - g_n \le 0, \quad \sigma_{cn} \le 0, \quad \sigma_{cn} G_n = 0 \\ \sigma_{cT} = 0 \end{array}\right\} \quad (\text{on } \Gamma_c, t) \tag{6} $$

where G_n is the current normal gap function. For the i^{th} contact pair on the indentation surface Γ_c, u_n is the normal component of the unilateral displacement, g_n is the initial gap measured along the outward normal, σ_{cn} is the normal component of the contact stress vector while σ_{cT} is the tangential component. Equation (6) describes boundary conditions at the indentation interface, such that, the first inequality represents the compatibility contact constraints, the second inequality states that no tensile normal stresses can be developed throughout the indentation interface, while the third condition implies that the indentation pressure can only be nonzero when there is contact. The last equation states that no tangential stress is developed throughout the indentation interface due to frictionless contact assumption.

The linear elastic response of the bulk of the thin film is assumed to obey the Hooke's law. On contrary, the linear viscoelastic behavior of the viscoelastic layer is modeled by Schapery's creep model as (Schapery 1969, 1984):

$$
\begin{aligned}
{}^{t}\varepsilon_{ij}^{B} &= (1+v)\left[D_o\,{}^{t}S_{ij}^{d} + \int_0^t \Delta D(t-\tau)\frac{d^{\tau}S_{ij}^{d}}{d\tau}d\tau\right]^{B} \\
&\quad + \frac{1}{3}\delta_{ij}(1-2v) \\
&\quad \left[D_o\,{}^{t}\sigma_{kk} + \int_0^t \Delta D(t-\tau)\frac{d^{\tau}\sigma_{kk}}{d\tau}d\tau\right]^{B} \left(\text{in } \Omega^{(3)},\ \text{t}\right)
\end{aligned}
\tag{7}
$$

where ${}^{t}\sigma_{kk}$, and ${}^{t}S_{ij}^{d}$ are used to denote the dilatational stress and the deviatoric stress tensors, respectively, D_o and $\Delta D(t)$ are the instantaneous and transient components of uniaxial creep compliance of linear viscoelasticity, respectively and δ_{ij} is a Kronecker-delta. The uniaxial transient compliance can be expressed using a Prony's series, such that:

$$
\Delta D(t) = \sum_{n=1}^{N} D_n\{1 - exp(-\lambda_n t)\} \tag{8}
$$

where D_n is the nth coefficient of the Prony's series, N is the number of repeated models in Prony's series, while λ_n is the nth retardation time.

The behavior of the surface S is treated by Gurtin–Murdoch (GM) surface elasticity model. According to this model, neglecting all rotation terms, as suggested by Mogilevskaya et al. (2008), the Lagrangian surface energy is given by Ru (2010):

$$
\begin{aligned}
\gamma &= \tau_s\left(1+\varepsilon_{\alpha\alpha}^{S}\right) + \frac{1}{2}(\lambda_s+\tau_s)\left(\varepsilon_{\alpha\alpha}^{S}\right)^2 + (\mu_s-\tau_s)\,\varepsilon_{\alpha\beta}^{S}\varepsilon_{\alpha\beta}^{S} \\
&\quad + \tau_s\frac{1}{2}|\nabla_s\mathbf{u}|\cdot|\nabla_s\mathbf{u}|
\end{aligned}
\tag{9a}
$$

Considering a state of plane strain, Eq. (9a) can be rewritten as, (Gad et al. 2014):

$$
\begin{aligned}
\gamma &= \tau_s\left(1+\varepsilon_{xx}^{S}\right) + \frac{1}{2}(\lambda_s+\tau_s)\left(\varepsilon_{xx}^{S}\right)^2 + (\mu_s-\tau_s)\left(\varepsilon_{xx}^{S}\right)^2 \\
&\quad + \frac{1}{2}\tau_s\left(u_{,x}^{s}+v_{,x}^{s}\right)^2
\end{aligned}
\tag{9b}
$$

where τ_s is the surface energy/tension, λ_S and μ_S are the two surface/interface elastic constants independent of the initial surface tension τ_s. It is noted from Eq. (9b) that the first three terms are dependent on the 2D surface infinitesimal strains ε^S, while the last term expresses the 2nd order displacement gradient.

The equilibrium conditions on the surface, surface constitutive relations and strain–displacement relationship, when specialized to the flat surface, are given by Gurtin et al. (1998)

$$
\sigma_{ij,j}^{s} + t_i^{s} + t_i^{o} = 0, \tag{10}
$$

$$
\sigma_{ij}^{s} = \tau_s\delta_{ij} + 2(\mu_s-\tau_s)\varepsilon_{ij}^{s} + \left(\tau_s+\lambda_s\right)\varepsilon_{kk}^{s}\delta_{ij} + \tau_s u_{i,j}^{s}, \quad i,j,k = 1,2 \tag{11}
$$

$$
{}^{t}\varepsilon_{ij}^{s} = \frac{1}{2}\left(u_{i,j}^{S} + u_{j,i}^{S}\right) \tag{12}
$$

where the superscript 'S' is used to denote the quantities corresponding to the surface and t^o denotes the traction exerted on the top side of the surface by the indenter (Indentation traction vector). By substituting (11) and (12) into (10), it leads to the equilibrium equations of the surface in terms of the surface displacement as shown below

$$
\mu_s u_{i,jj}^{s} + (\tau_s+\lambda_s)u_{j,ji}^{s} + t_i^{s} + t_i^{o} = 0 \tag{13}
$$

3 Finite element formulation

This section presents the finite element model of nanoindentation problem of viscoelastic layer coated with an elastic thin film taking into account the influence of surface energy. To do this, firstly, the viscoelastic constitutive relations are recast into a recursive incremental form suitable for the FE implementation. Secondly, based on the finite element discretization, the incremental equilibrium equations are derived.

3.1 The recursive form of viscoelastic constitutive equations

Generally, working with the constitutive Eq. (7) leads to the requirement of solving a set of integrals (Zocher et al. 1997). To overcome this difficulty the constitutive equations are transformed into a recursive incremental form, which will be quite amenable to implement into a FE model (Haj-Ali and Muliana 2004). Once the time domain is divided into discrete time intervals Δt, such that $t_{n+1} = t_n + \Delta t$. Recalling Eq. (7), the strain at time $t + \Delta t$ can be expressed as:

$$
{}^{t+\Delta t}\varepsilon_{ij}^{B} = (1+v)\left(D_o\, {}^{t+\Delta t}S_{ij}^{d} + \int_0^{t+\Delta t} \sum_{n=1}^{N} D_n \left[1 - exp\{-\lambda_n(t+\Delta t-\tau)\}\right] \frac{d^{\tau}S_{ij}^{d}}{d\tau} d\tau \right)^{B}
$$

$$
+ \frac{1}{3}\delta_{ij}(1-2v)\left(D_o^{t+\Delta t}\sigma_{kk} + \int_0^{t+\Delta t} \sum_{n=1}^{N} D_n \left[1 - exp\{-\lambda_n(t+\Delta t-\tau)\}\right] \frac{d^{\tau}\sigma_{kk}}{d\tau} d\tau \right)^{B} \quad \left(\text{in } \Omega^{(3)},\ \text{t}\right) \tag{14}
$$

Assuming that both ${}^{\tau}S_{ij}^{d}$ and ${}^{\tau}\sigma_{kk}$ change linearly over the current time increment, the evaluation of the integrations in Eq. (14) yields, (Mahmoud et al. 2013):

To obtain the current incremental strain:

$$
{}^{t+\Delta t}\Delta\varepsilon_{ij}^{B} = {}^{t+\Delta t}\,\varepsilon_{ij}^{B} - {}^{t}\,\varepsilon_{ij}^{B} \tag{17}
$$

$$
{}^{t+\Delta t}\varepsilon_{ij}^{B} = (1+v)\left[D_o\, {}^{t+\Delta t}S_{ij}^{d} + {}^{t+\Delta t}\,S_{ij}^{d} \sum_{n=1}^{N} D_n - \sum_{n=1}^{N} D_n \left(exp(-\lambda_n\Delta t)\, {}^{t}q_{n_{ij}} + \frac{\left\{ {}^{t+\Delta t}S_{ij}^{d} - {}^{t}\,S_{ij}^{d} \right\}}{\lambda_n \Delta t}\{1 - exp(-\lambda_n\Delta t)\} \right) \right]^{B} +
$$

$$
\frac{1}{3}\delta_{ij}(1-2v)\left[D_o\, {}^{t+\Delta t}\sigma_{kk} + {}^{t+\Delta t}\,\sigma_{kk} \sum_{n=1}^{N} D_n - \sum_{n=1}^{N} D_n \left(exp(-\lambda_n\Delta t)\, {}^{t}q_{n_{kk}} + \frac{\left\{ {}^{t+\Delta t}\sigma_{kk} - {}^{t}\,\sigma_{kk} \right\}}{\lambda_n \Delta t}\{1 - exp(-\lambda_n\Delta t)\} \right) \right]^{B}
$$

$$
\left(\text{in } \Omega^{(3)},\ \text{t}\right) \tag{15}
$$

With

$$
q_{n_{ij}} = \int_0^{t} exp\{-\lambda_n(t-\tau)\} \frac{d\,{}^{\tau}S_{ij}^{d}}{d\tau} d\tau, \quad \text{and}
$$

$$
{}^{t}q_{n_{kk}} = \int_0^{t} exp\{-\lambda_n(t-\tau)\} \frac{d\,{}^{\tau}\sigma_{kk}}{d\tau} d\tau \tag{16}
$$

Substituting from Eq. (15) into Eq. (17), the incremental strain can be expressed as:

$$
{}^{t+\Delta t}\Delta\varepsilon_{ij}^{B} = \left\{ (1+v) D_o\, {}^{t+\Delta t}\Delta S_{ij}^{d} + \frac{1}{3}\delta_{ij}(1-2v) D_o\, {}^{t+\Delta t}\Delta\sigma_{kk} \right\}^{B}
$$

$$
- \sum_{n=1}^{N} D_n \left\{ \left[exp(-\lambda_n\Delta t) - 1 \right] \left((1+v)\, {}^{t}q_{n_{ij}} + \frac{1}{3}\delta_{ij}(1-2v)\, {}^{t}q_{n_{kk}} \right) \right\}^{B}
$$

$$
+ \sum_{n=1}^{N} D_n \left\{ 1 - \left(\frac{1 - exp(-\lambda_n\Delta t)}{\lambda_n\Delta t} \right) \right\} \left((1+v)\, {}^{t+\Delta t}\Delta S_{ij}^{d} + \frac{1}{3}\delta_{ij}(1-2v)\, {}^{t+\Delta t}\Delta\sigma_{kk} \right)^{B} \left(\text{in } \Omega^{(3)},\ \text{t}\right) \tag{18}
$$

Based on the incremental form expressed in Eq. (18) the approximate incremental stress, ${}^{t+\Delta t}\Delta\sigma_{ij}$ can be expressed as:

$$ {}^{t+\Delta t}\Delta\sigma_{ij}^{B} = \frac{1}{D_o + {}^{t+\Delta t}\mathrm{T}_n}\left(\frac{{}^{t+\Delta t}\Delta\varepsilon_{ij}}{1+\nu} - {}^{t+\Delta t}\Delta\varepsilon_{kk}\delta_{ij}\left[\frac{\nu}{(1-2\nu)(1+\nu)}\right] + \sum_{n=1}^{N} {}^{t+\Delta t}\alpha_n\left[{}^{t}q_{n_{ij}} + \frac{1}{3}\delta_{ij}\,{}^{t}q_{n_{kk}}\right]\right)^{B} \quad \left(\text{in } \Omega^{(3)},\ \text{t}\right) \tag{19} $$

with

$$ {}^{t+\Delta t}\mathrm{T}_n = \sum_{n=1}^{N} D_n\left(1 - \frac{1 - exp(-\lambda_n\Delta t)}{\lambda_n\Delta t}\right), \qquad {}^{t+\Delta t}\alpha_n = D_n\left\{exp(-\lambda_n\Delta t) - 1\right\} \tag{20} $$

Equation (19) can be rewritten in the following form:

$$ {}^{t+\Delta t}\Delta\sigma_{ij}^{B} = {}^{t+\Delta t}C_{ijrs}^{B}\,{}^{t+\Delta t}\Delta\varepsilon_{rs}^{B} + {}^{t+\Delta t}\Delta\sigma_{ij}^{h^B} \tag{21} $$

where ${}^{t+\Delta t}\Delta\sigma_{ij}^{h^B}$ is the stress increment which expresses the viscoelastic material history.

3.2 Incremental finite element equilibrium equations

The finite element equilibrium equations can be obtained by applying the principle of virtual work. The variational form of the nanoindentation problem incorporating the surface energy effect can be expressed as:

$$ \int_{\Omega_B} \delta\varepsilon_{ij}^{B^T}\,\sigma_{ij}^{B}d\Omega + \int_{\Omega_s} \delta\varepsilon_{ij}^{s^T}\,\sigma_{ij}^{s}d\Omega - \int_{\Gamma_f} \delta u_i^T\,F_i\,d\Gamma + \int_{\Gamma_c} \delta(\Lambda_n G_n)d\Gamma = 0 \tag{22} $$

where the 1st term is the usual virtual work developed by the internal stresses within the bulk domains, while the 2nd term denotes to the virtual work due to surface stresses, finally, the last two terms represent the virtual work done by the external forces and contact forces, respectively.

To develop the finite element equilibrium equations, both the bulk of the indenter and the indented domains are discretized into finite elements while the surface of the indented domain is discretized into surface elements adhered to the boundary element of the bulk, as shown in Fig. 2. On the other hand, the contact interface is modeled through node to segment contact approach (Wriggers 2006). Based on this idealization of the contact interface, the contact force at the master node A should be balanced by equivalent nodal forces at slave segment nodes A_1 and A_2 as shown in Fig. 3. Thus one can write:

$$ {}^{t+\Delta t}\tilde{\Lambda}_{n_{A_1}} = -\frac{1}{2}\left\{1 - {}^{t+\Delta t}\xi_P\right\}{}^{t+\Delta t}\tilde{\Lambda}_{nA} \qquad \text{and} $$
$$ {}^{t+\Delta t}\tilde{\Lambda}_{n_{A_2}} = -\frac{1}{2}\,{}^{t+\Delta t}\xi_P\,{}^{t+\Delta t}\tilde{\Lambda}_{n_A}, \tag{23} $$

where ${}^{t+\Delta t}\xi_P$ is a parameter identifies the location of the physical contact point on the slave segment.

Substituting from Eq. (21) into Eq. (22) the first integral yields:

$$ \int_{\Omega^B} \delta\varepsilon^{B^T}\,\sigma^{B}d\Omega = \int_{\Omega_B} \delta\,{}^{t+\Delta t}\Delta u^T B^T\,{}^{t+\Delta t}C\,B\,{}^{t+\Delta t}\Delta u\,d\Omega + \int_{\Omega_B} \delta\,{}^{t+\Delta t}\Delta u^T B^T\,{}^{t}\sigma^{B}\,d\Omega + \int_{\Omega_B} \delta\,{}^{t+\Delta t}\Delta u^T B^T\,{}^{t+\Delta t}\Delta\sigma^{h^B}\,d\Omega \tag{24a} $$

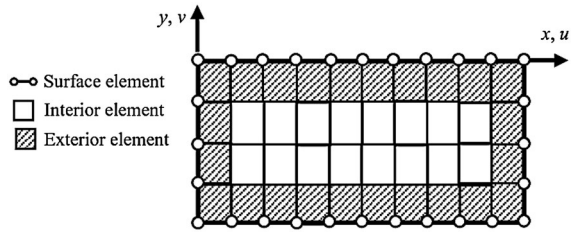

Fig. 2 Schematic diagram of mesh map of solid containing surface elements

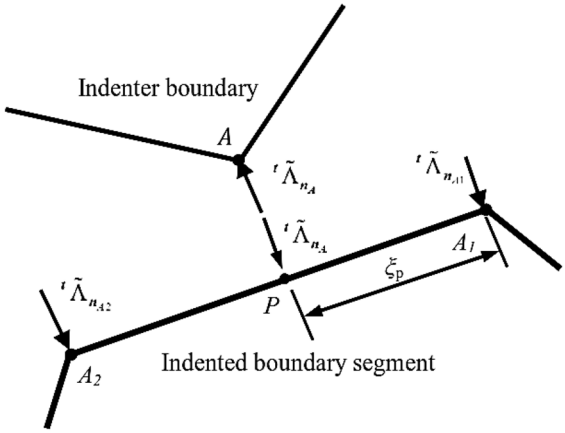

Fig. 3 Contact forces at a master node A and the corresponding indented body segment nodes A_1 and A_2

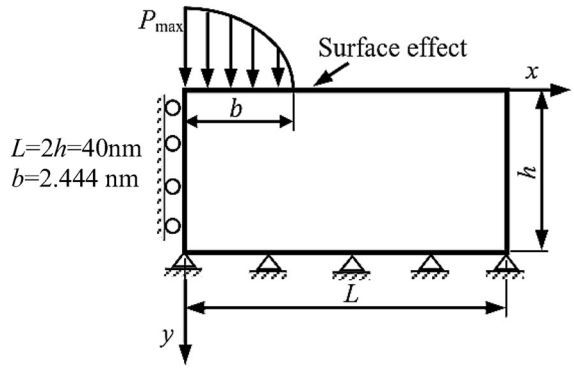

Fig. 4 Block under Hertzian distributed pressure

where $\boldsymbol{B}$ is the strain -displacement transformation matrix.

The second and third integrals of the R.H.S. of (24a) represent the virtual work due to internal stresses and material damping. By the same way, the contribution of the surface energy effect can be obtained as:

$$\int_{\Omega_s} \delta\varepsilon^{s^T}\sigma^s d\Omega = \int_{\Omega_s} \delta^{\,t+\Delta t}\Delta u^{sT} B'^{sT\,t+\Delta t} C'^s B'^{s\,t+\Delta t}\Delta u^s \, d\Omega + \int_{\Omega_s} \delta^{\,t+\Delta t}\Delta u^{sT} B^{sT\,t}\sigma^s \, d\Omega + \int_{\Omega_s} \delta^{\,t+\Delta t}\Delta u^{sT} B^{sT}\tau_s \, d\Omega \tag{24b}$$

where C^s, B'^S and B^s are the surface stress–strain relationship matrix and strain–displacement transformation matrices, respectively. Using Eqs. (11) and (12), theses matrices can be obtained as:

$$C'^s = \begin{bmatrix} \lambda_s+2\mu_s & 0 \\ 0 & \tau_s \end{bmatrix} \quad B'^s = \frac{1}{L}\begin{bmatrix} -1 & 0 & 1 & 0 \\ 0 & -1 & 0 & 1 \end{bmatrix}$$
$$B^s = \frac{1}{L}\begin{bmatrix} -1 & 0 & 1 & 0 \end{bmatrix} \tag{24c}$$

The third integral of the R.H.S. of (24b) represents the virtual work due to surface tension.

The third integral in Eq. (22) which represents the virtual work due to external surface traction can be evaluated as:

$$-\int_{\Gamma_f} \delta u^T F d\Gamma = -\int_{\Gamma_f} \delta^{\,t+\Delta t}\Delta u^{T\,t+\Delta t} F \, d\Gamma \tag{24d}$$

Lastly the contribution of the indentation traction can be evaluated by substituting from Eqs. (6) and (23) into the last term in Eq. (22) yields:

$$\int_{\Gamma_c} \delta(\Lambda_n G_n) d\Gamma = \int_{\Gamma_c} \delta\Lambda_n G_n \, d\Gamma + \int_{\Gamma_c} \Lambda_n \delta G_n \, d\Gamma = \int_{\Gamma_c} \delta^{\,t+\Delta t}\Delta\Lambda_n^T \left({}^tC_n^{T\,t+\Delta t}\Delta u - {}^t g_n\right) d\Gamma + \int_{\Gamma_c} \delta^{\,t+\Delta t}\Delta u_n^T \left({}^t\Lambda_n + {}^tC_n{}^{t+\Delta t}\Delta\Lambda_n\right) d\Gamma \tag{24e}$$

Substituting from Eqs. (24a–24e) and setting the coefficients of $\delta^{\,t+\Delta t}\Delta u$ and $\delta^{\,t+\Delta t}\Delta\Lambda_n$ to be zero the overall equilibrium equations for nanoindentation problems including the surface energy effect can be written in the following matrix form:

$$ {}^{t}\begin{bmatrix} [K_B + K_s] & [C_n] \\ [C_n]^T & [0] \end{bmatrix} {}^{t+\Delta t}\begin{Bmatrix} \Delta u \\ \Delta \Lambda_{nA} \end{Bmatrix} = \begin{Bmatrix} {}^{t+\Delta t}\{F\} + {}^{t+\Delta t}\{F_s\} - {}^{t}\{F^B_{int}\} - {}^{t}\{F^s_{int}\} + {}^{t}[C_n]\ {}^{t}\{\Lambda_{nA}\} \\ {}^{t}\{G\} \end{Bmatrix} \tag{25} $$

where

$$ \begin{aligned} [K_B] &= \int_{\Omega_B} [B]^T [C][B] d\Omega, \qquad {}^{t}\{F^B_{\text{int}}\} \\ &= \int_{{}^{t}\Omega_B} [B]^{Tt}\{\sigma\}^B d\Omega + \int_{{}^{t}\Omega_B} [B]^{Tt}\{\Delta\sigma^h\}^B d\Omega, \\ \text{and } {}^{t}\{F^s_{\text{int}}\} &= \int_{{}^{t}\Omega_s} [B^s]^{Tt}\{\sigma^s\} d\Omega \end{aligned} \tag{26} $$

model eliminates both geometrical and boundary complexity considerations encountered in most theoretical studies; (Zhou and Gao 2013; Long et al. 2012; Long and Wang 2013). For the sake of validation, the developed indentation model should be tested and compared. In the real nanoindentation experiment, real surfaces and interfaces may have much more complicated morphologies and microstructures which are different from the ideal surfaces considered in in most developed theoretical studies which are assumed

$$ \begin{aligned} [K_S] &\equiv \int_{\Omega_s} [B'^s]^T [C'^s][B'^s] d\Omega = \frac{b}{L}\begin{bmatrix} (\lambda_s{+}2\mu_s) & 0 & -(\lambda_s{+}2\mu_s) & 0 \\ 0 & \tau_s & 0 & -\tau_s \\ -(\lambda_s{+}2\mu_s) & 0 & (\lambda_s{+}2\mu_s) & 0 \\ 0 & -\tau_s & 0 & \tau_s \end{bmatrix} \\ \text{and } {}^{t+\Delta t}\{F_s\} &= \int_{\Omega_s} [B^s]^T \tau_s d\Omega = \begin{Bmatrix} b\tau_s \\ 0 \\ -b\tau_s \\ 0 \end{Bmatrix} \end{aligned} \tag{27} $$

where b is the surface element thickness and L is the element length, ${}^{t+\Delta t}[C_n]$ is a matrix operator of all active contact constraints. This operator matrix includes the constraints of compatible boundary displacements due to contact after time t. This matrix operator can be expressed as:

$$ {}^{t+\Delta t}[C_n] = \begin{Bmatrix} {}^{t}\tilde{n}^T & -\frac{1}{2}{}^{t}\tilde{n}^T\left(1 - {}^{t}\xi_P\right) & -\frac{1}{2}{}^{t}\tilde{n}^{Tt}\xi_P \end{Bmatrix}^T \tag{28} $$

4 Verification of the model

The developed model is implemented into a displacement–based 2D nonlinear FE program. This integrated to be smooth and clean. In addition to surface roughness effects, the real tip shape of the indenter, the interactions with the environment (e.g., the change of temperature and moisture) and the adhesion force throughout the indentation interface are considered in these experiments. All theses sources increase the systematic error between the experimental responses and the numerical predictions, (Chen and Diebels 2014). Consequently, for the sake of the model validation, consider a 2D plane strain analysis of a block subjected Hertzian pressure distribution, as shown in Fig. 4. The pressure profile is described by $P(x) = (P_{max}/b)\sqrt{b^2 - x^2}$, where P_{max} is the maximum pressure intensity and b is the half load span. Material properties for the bulk and surface are defined

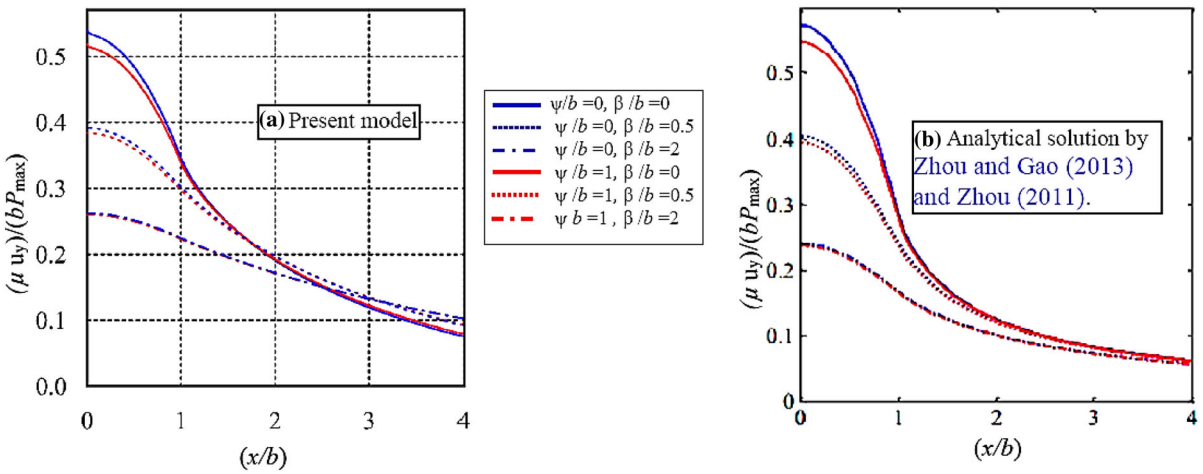

Fig. 5 Non-dimensional vertical displacement at the loaded surface **a** present FE model, **b** Zhou and Gao (2013) and Zhou (2011)

by the dimensionless constants; $\beta = \tau_s/\mu$ and $\psi = (\lambda_s + 2\ \mu_s)/\mu$, where μ is the shear modulus of the bulk material.

As shown in Fig. 5, the obtained results by the developed FE model for the non–dimensional vertical displacement at the loaded surface are in good agreement with the analytical solution obtained by Zhou (2011) and Zhou and Gao (2013). The deviation between the obtained results and those reported in the above references may be explained by the half space assumption on which the analytical solution is based upon.

5 Numerical results

Within this section the effectiveness of the developed model is demonstrated by solving two different nanoindentation problems with different indenter profile and different material flexibility. In each problem, the effects of the surface/interface energy and the second order gradient of surface displacement on the nanoindentation response are investigated. In the following analysis, three different models are discussed; the first is based on the classical linear elasticity theory (classical) and the other two models accounted for surface energy effects with and without the second order displacement gradient term; (SL) and (SN), respectively.

5.1 Nanoindentation of elastically-layered viscoelastic layer by a cylindrical rigid indenter

The influence of surface energy on the quasistatic plane strain nanoindentation response of an elastically-layered viscoelastic layer indented by a rigid cylindrical indenter is investigated, as shown in Fig. 6. The indenter is subjected to a prescribed constant downward displacement $D_p = 0.025$ nm (relaxation load) over a time period [0, 200] s. The indented body is composed of an elastic film of 1 nm thickness and a viscoelastic layer of 9 nm thickness. Both bulk and surface material constants of the elastic film are as follows $D^B = 17.\ 8 \times 10^{-6}$ MPa^{-1}, $\nu =$

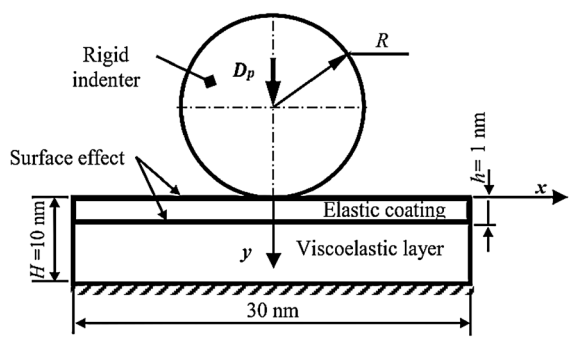

Fig. 6 Nanoindentation of composite layer by a rigid cylindrical indenter

Table 1 Coefficients of the Prony's series for the viscoelastic material (Lai and Bakker 1996)

N	D_0	D_1	D_2	D_3	D_4	D_5	D_6	D_7	D_8	D_9
$D_n \times 10^{-6}$ (MPa^{-1})	270.90	23.6	5.6602	14.8405	18.8848	28.5848	40.0569	60.4235	79.6477	162.179
λ_n (s^{-1})	0	10^{-1}	10^{-2}	10^{-3}	10^{-4}	10^{-5}	10^{-6}	10^{-7}	10^{-8}	10^{-9}

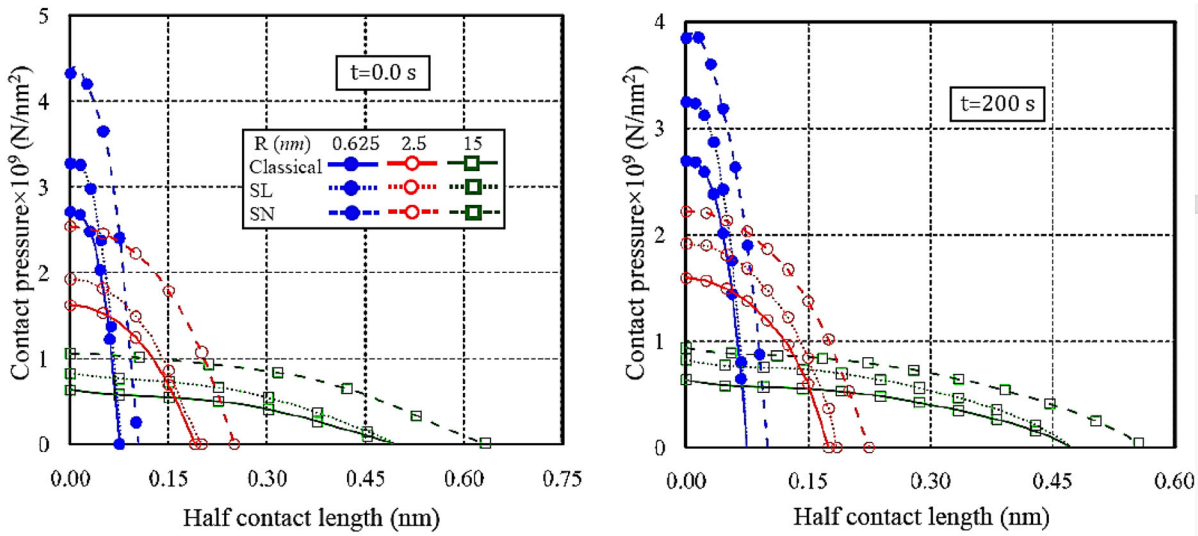

Fig. 7 Contact pressure distributions for different indenter radius at two different time instants

0.25, $\tau_s = 0.11$ N/mm, $\mu_s = 8$ N/mm, $\lambda_s = 7$ N/mm, (Gurtin and Murdoch 1975). The transient component of the creep compliance of viscoelastic layer is expressed by nine elements of the Prony's series with coefficients in Table 1 and Poisson ratio of 0.4, (Lai and Bakker 1996). The size dependency on the surface energy effect is examined considering different indenter radii keeping the same indentation depth, D_p.

Distributions of the contact pressure for classical (without surface effect), linear and nonlinear analyses with surface effect (SL) and (SN), respectively for different indenter radii at two different time instants, are presented in Fig. 7. It is clear that the surface energy affects both the contact pressure and the extent of contact area. Due to the influence of surface stresses, higher values of the instantaneous contact pressures are obtained with larger extent of the contact area. This implies that the presence of the surface stresses make the material more stiff. These results qualitatively agree well with that reported in Long et al. (2012). Incorporating the second order displacement gradient term into the surface constitutive relation (SN) makes the material more stiff thus more increase in the contact pressure with larger extent of contact area is obtained comparing with the corresponding linear (SL) case. Moreover the indenter size has a significant effect on the nanocontact response. Increasing the indenter radius, lower values of the contact pressure with larger extent of the contact area are obtained. Also, the difference between the classical and the nonclassical contact pressures is decreased with increasing the indenter radius. Consequently the effect of surface energy on the mechanical response of the contacting system discards with increasing the indenter size. For all indenter radii and with time marching, the equivalent stiffness of the viscoelastic layer is decreased due to the damping effect of the viscoelastic material. Consequently, under such loading pattern (relaxation load type), the contact pressures are decreased with time.

Figure 8 shows the variations of the central contact pressures with time for different indenter radius. It is noted that both the central contact pressure and its relaxation rate are increased with the presence of

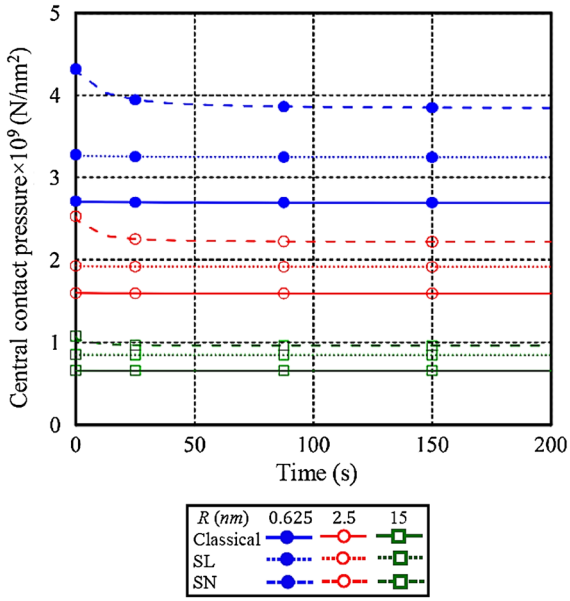

Fig. 8 Variation of the central contact pressure with time for different indenter radius

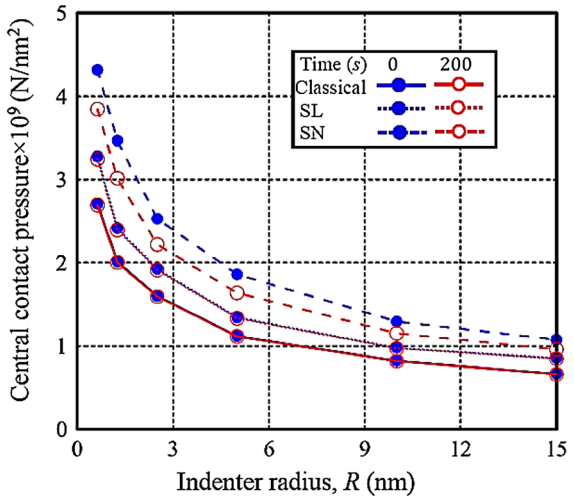

Fig. 9 Variation of the central contact pressure with the indenter radius for two different time instants

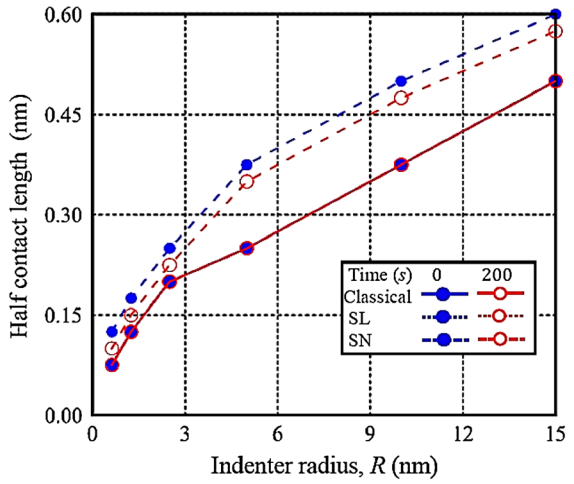

Fig. 10 Variation of the half contact length with the indenter radius for two different time instants

surface energy. On the other hand, the indenter radius has a remarkable effect on the central contact pressures and its relaxation rates. Both the central contact pressure and its relaxation rate are decreased with increasing the indenter size. The relative percentage ratio between the instantaneous central contact pressure and that at the final time instant, $[(P_{ts} - P_{tf})/P_{ts}]$ % reaches 0.66 % for $R = 0.625$ nm and 0.424 % for $R = 15$ nm for the classical material behavior. This ratio is increased with the presence of surface energy (SL) and reaches 1 % for $R = 0.625$ nm and 0.61 % for $R = 15$ nm. Moreover, more increase in the relaxation rate is obtained by incorporating the second order gradient term into the surface constitutive relation (SN). The percentage ratio $[(P_{ts} - P_{tf})/P_{ts}]$ % for SN reaches 10.93 % for $R = 0.625$ nm and 10.87 % for $R = 15$ nm.

For more illustrations, the influence of the indenter radius on the central contact pressure and the extent of the contact area is shown Figs. 9 and 10, respectively. It is noticeable that the difference between the classical and the nonclassical central contact pressure decreases with increasing the indenter radius. Moreover, increasing the indenter radius produces lower values of the central contact pressure and larger extent of the contact area. With time marching, lower values of the central contact pressure are obtained specially with SN case due to the surface effect and the viscoelastic material damping.

The effect of the surface energy on the vertical displacement thorough the indentation interface at different indenter radii for two different time instants are depicted in Fig. 11. It is noted that surface energy affects both the magnitude and the decaying rate of the vertical displacement throughout the layer length. It is clear that surface effect produces vertical displacement with slower decaying rate throughout the layer length compared with the corresponding classical

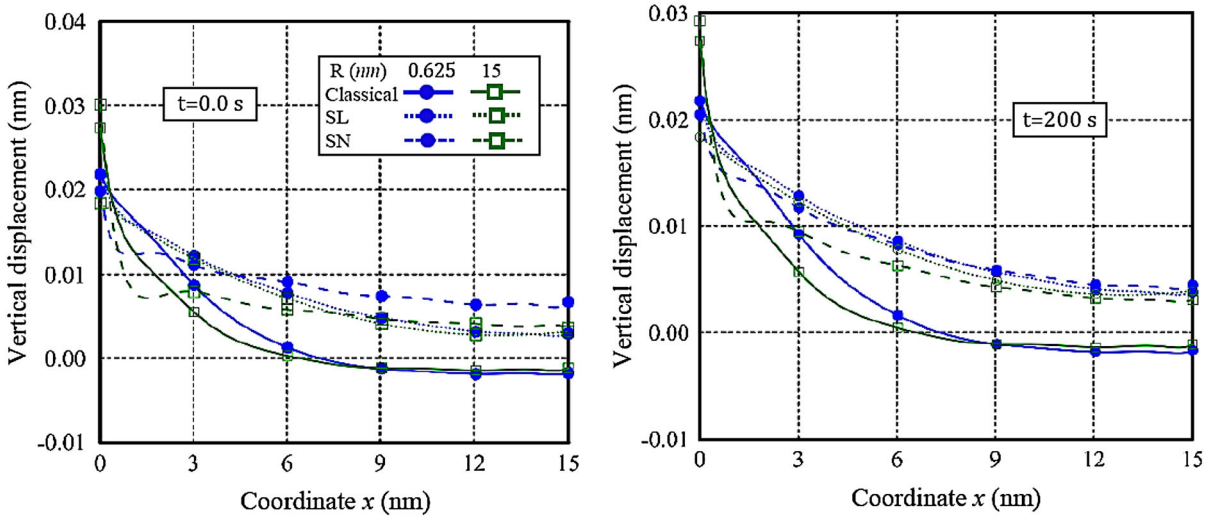

Fig. 11 Vertical displacement distributions throughout the contact interface for different indenter radius at two different time instants

case. Moreover incorporating the second order displacement gradient term into the surface constitutive relation (SN) decreases the material flexibility and thus producing vertical displacements with slower decaying rate throughout the layer length compared with the corresponding linear (SL) case. With time marching, due to the viscoelastic damping with surface energy, higher creep rate of the displacement is obtained while the classical case produces constant displacement at all-time instants. This is due to the additional creep load (surface tension) associated with surface energy. It is also noticed that the indenter size significantly affects the vertical displacement and its decaying rate throughout the layer length. Increasing the indenter radius results in a decrease in the vertical displacement with faster decaying rate throughout the layer length.

5.2 Indentation of an elastically-layered viscoelastic substrate with a viscoelastically-layered elastic block

Consider the indentation of an elastically-layered viscoelastic substrate with a viscoelastically-layered elastic block under the action of uniform pressure of intensity, $Q_o = 8 \times 10^{-10}$ N/nm^2 as shown in Fig. 12. This type of problems pertains to a conforming contact without friction. Due to the symmetry about the vertical axis, only the right half of the domain is needed to be modelled with the

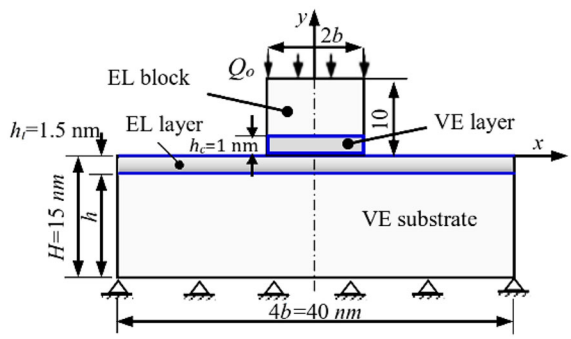

Fig. 12 Indentation of an elastically-layered VE substrate by a viscoelastically-layered VE block

corresponding geometry, loads and boundary conditions. The elastic material characteristics reported in Gurtin and Murdoch (1975) are considered for both bulk and surface material properties of the elastic block and the surface layer bonded to the viscoelastic substrate while the viscoelastic material of the viscoelastic layer bonded to the elastic block and the viscoelastic substrate is depicted in Table 1. It is important to mention that, the effect of surface energy at the upper surface of the elastic block and upper surface of the elastic layer, bonded to the viscoelastic substrate, on the contact configuration is investigated.

The contact pressure profiles for the classical, SL and SN models are depicted in Fig. 13. It is noticed that the surface energy has a significant effect on the contact pressure profile throughout the indentation

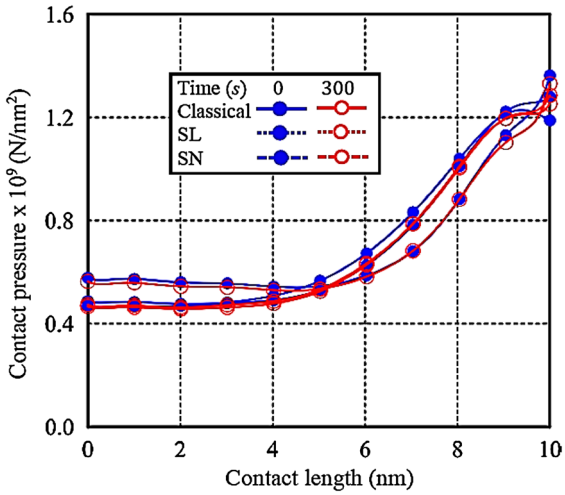

Fig. 13 Contact pressure distributions at two different time instants for different material responses

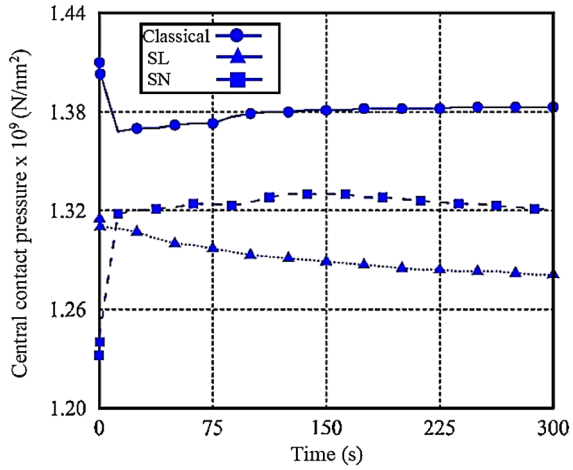

Fig. 14 Variation of the central contact pressure with time for different material responses

interface. The surface effect increases the material stiffness and produces an additional tangential force vector owing to the initial surface tension τ_s thus increases the contact pressure at the right edge of the block and decreases it at its center. Moreover, incorporating the second order displacement gradient term into the surface constitutive relations results in a more increase in the contact pressure on the right edge of the block and a more decreases at its center. With time marching, due to the displacement creep the contact area is slightly increase which results in a slight decrease in the contact pressure throughout the contact interface.

Variations of the central contact pressures with time for different material responses are depicted in Fig. 14. It is noted that the surface energy affects both the magnitudes and the relaxation rate of the central contact pressure. The relative percentage ratio between the instantaneous central contact pressure and that at the final time instant $[(P_{ts} - P_{tf})/P_{ts}]$ % is 2.57 % for the classical response. This ratio increases with the presence of surface energy and reaches 4.2 % for SL response. Incorporating the second order displacement gradient term into the surface constitutive relations results in an increase in the central contact pressure at the beginning of the time domain due to the increase in the material stiffness associated with the surface effect. With time marching, owing to the viscoelastic material damping, the central contact pressure decreases with time.

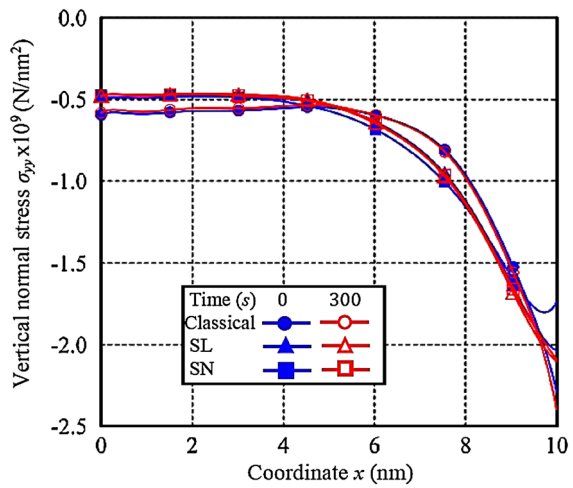

Fig. 15 Vertical normal stress distributions throughout the contact interface at two different time instants for different material responses

Distributions of the normal stress, σ_{yy} at the indentation interface are illustrated in Fig. 15. It is noticeable that for all models, i.e. classical, SL, and SN, the normal stresses, σ_{yy} have the same trend of the corresponding contact pressure. It is also found that the normal stress component, σ_{yy} is significantly affected by the presence of the surface energy. Variations of the central vertical normal stress, σ_{yy} at the contact interface with time for different material responses are shown in Fig. 16. As detected in the contact pressure variation with time, it is noted that the

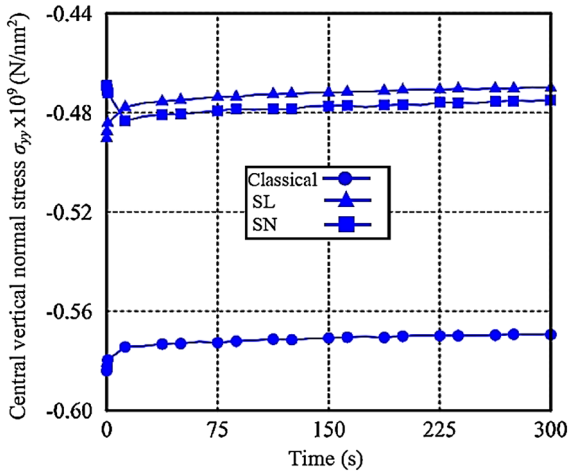

Fig. 16 Variation of the central vertical stress with time for different material responses

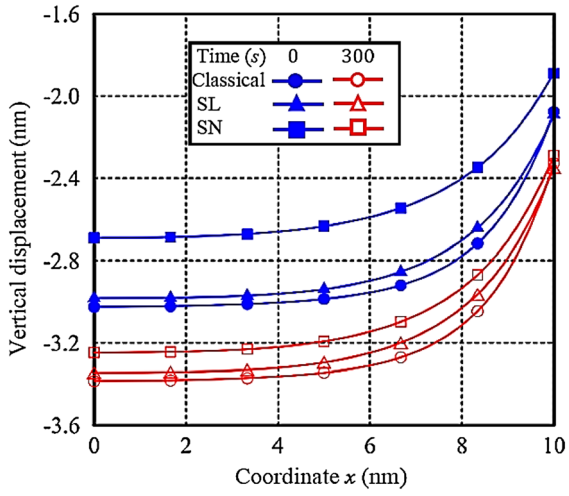

Fig. 17 Vertical displacement at the contact interface for two different time instants for different material responses

surface energy also affects the magnitudes and the relaxation rate of the vertical normal stress component with time.

Figure 17 shows the profiles of the vertical displacement at the contact interface. It is depicted that the surface energy results in a distinct decrease in the absolute vertical displacement throughout the indentation interface. It is also notable that the second order displacement gradient term has a remarkable effect on the profile of the vertical displacement at the indentation interface. With time marching, a significant increase in the absolute vertical displacement is noted

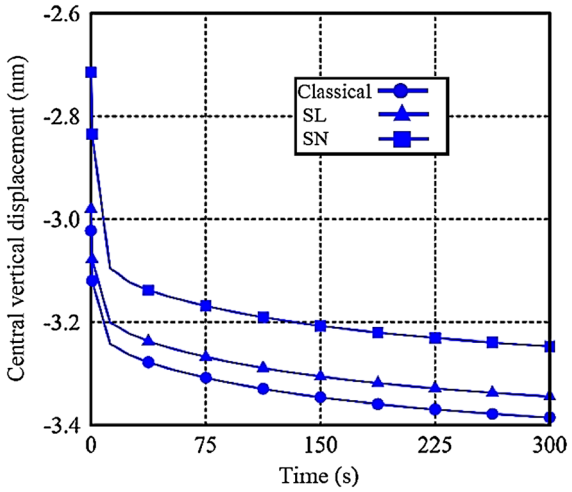

Fig. 18 Variation of the absolute central vertical displacement with time for different material responses

due to the viscoelastic material damping under such creep loading. The presence of the surface energy effect increases the creep in the displacement due to the additional creep load associated with the surface tension, τ_s.

Variations of the central vertical displacement component with time for different material responses are illustrated in Fig. 18. It is noted that both the magnitude and the creep rate of the central vertical displacement component are significantly affected by the presence of surface energy. The absolute relative percentage ratio between the instantaneous central vertical displacement component at the indentation interface and that at the final time instant $|(u_{yts} - u_{ytf})/u_{yts}|$ % is 12.0 % for the classical response. This ratio increases with the presence of surface effect and reaches 12.24 % for SL response. Moreover, incorporating the second order displacement gradient term into the surface constitutive relation increases this percentage ratio; 19.6 % for the SN response.

6 Conclusions

In the context of an integrated nonlinear viscoelastic contact mechanics, a computational model to investigate the nanoindentation response of elastically-layered viscoelastic solids, is developed. The developed model accounts for surface effects by adopting the complete Gurtin–Murdoch surface elasticity model. The

developed integrated model consists of two consecutive parts. The first one stands for solution of the contact problem of the indenter and the indented continuum to determine the contact pressure distribution and the extension of contact area. The second part exploits the results of the contact model to investigate the indentation response of an elastic/viscoelastic continuum subjected to the contact pressure distribution. In both parts of the model the surface energy effect has been taken into consideration. The frictionless contact constraints are established by using the Lagrange multiplier method. The Schapery's single integral creep model is used to model the linear viscoelastic behavior. The transient component in the creep function is assumed to be expanded by a Prony's series. The equilibrium configuration is obtained through Newton–Raphson iterative procedure. The developed model is flexible to deal with different indenter geometries with different material flexibility. The model is verified and applied to detect the quasistatic nanoindentation response of two different indentation problems with different geometry, different material flexibility, loading condition (i.e. relaxation or creep). The following findings are concluded from the obtained results.

- Surface energy has a remarkable effect on the quasistatic nanoindentation response of elastically-layered viscoelastic solids. This effect decreased with increasing the indenter size.
- Both the contact pressure profile and the extension of the contact area throughout the indentation interface are strongly influenced with the presence surface energy effect.
- Both stress relaxation and deformation creep rates are significantly affected with the presence of surface energy. These rates are increased with the presence of the surface energy.
- The second order displacement gradient term in the surface constitutive relation strongly affect the quasistatic indentation behavior of elastically-layered viscoelastic solids.

References

Beegan, D., Chowdhury, S., Laugier, M.T.: Comparison between nanoindentation and scratch test hardness (scratch hardness) values of copper thin films on oxidised silicon substrates. Surf. Coat. Technol. **201**, 5804–5808 (2007)

Cammarata, R.C.: Surface and interface stress effects in thin films. Prog. Surf. Sci. **46**, 1–38 (1994)

Cammarata, R.C.: Surface and interface stress effects on interfacial and nanostructured materials. Mater. Sci. Eng. A **237**, 180–184 (1997)

Chen, W.Q., Zhang, C.: Anti-plane shear Green's functions for an isotropic elastic half-space with a material surface. Int. J. Solids Struct. **47**(11), 1641–1650 (2010)

Chen, Z., Diebels, S.: Nanoindentation of soft polymers: modeling, experiments and parameter identification. Tech. Mech. **34**(3–4), 166–189 (2014)

Dingreville, R., Qu, J., Cherkaoui, M.: Surface free energy and its effect on the elastic behavior of nanosized particles, wires and films. J. Mech. Phys. Solids **53**, 1827–1854 (2005)

Duan, H.L., Wang, J., Huang, Z.P., Karihaloo, B.L.: Eshelby formalism for nano-inhomogeneities. Proc. R. Soc. A **461**, 3335–3353 (2005)

Fischer, F.D., Waitz, T., Vollath, D., Simha, N.K.: On the role of surface energy and surface stress in phase-transforming nanoparticles. Prog. Mater. Sci. **53**, 481–527 (2008)

Gad, A.I., Mahmoud, F.F., Alshorbagy, A.E., Ali-Eldin, S.S.: Finite element modeling for elastic nano-indentation problems incorporating surface energy effect. Int. J. Mech. Sci. **84**, 158–170 (2014)

Gao, W., Yu, S., Huang, G.: Finite element characterization of the size dependent mechanical behaviour in nanosystems. Nanotechnology **17**, 1118–1122 (2006)

Gurtin, M.E., Murdoch, A.I.: A continuum theory of elastic material surfaces. Arch. Ration. Mech. Anal. **57**, 291–323 (1975)

Gurtin, M.E., Murdoch, A.I.: Surface stress in solids. Int. J. Solids Struct. **14**, 431–440 (1978)

Gurtin, M.E., Weissmüller, J., Larché, F.: A general theory of curved deformable interfaces in solids at equilibrium. Philos. Mag. A **78**, 1093–1109 (1998)

Hainsworth, S.V., Page, T.F.: Nanoindentation studies of the chemomechanical effect in sapphire. J. Mater. Sci. **29**, 5529–5540 (1994)

Haj-Ali, R.M., Muliana, H.A.: Numerical finite element formulation of the Schapery nonlinear viscoelastic material model. Int. J. Numer. Methods Eng. **59**(1), 25–45 (2004)

He, L.H., Lim, C.W.: Surface green function for a soft elastic half-space: influence of surface stress. Int. J. Solids Struct. **43**, 132–143 (2006)

He, L.H., Lim, C.W., Wu, B.S.: A continuum model for size dependent deformation of elastic films of nano-scale thickness. Int. J. Solids Struct. **41**, 847–857 (2004)

Huang, D.W.: Size dependent response of ultra-thin films with surface effects. Int. J. Solids Struct. **45**, 568–579 (2008)

Huang, G.Y., Yu, S.W.: Effect of surface elasticity on the interaction between steps. J. Appl. Mech. **74**, 821–823 (2007)

Intarit, P., Senjuntichai, T., Rajapakse, R.K.N.D.: Dislocations and internal loading in a semi-infinite elastic medium with surface stresses. Eng. Fract. Mech. **77**, 3592–3603 (2010)

Intarit, P., Senjuntichai, T., Rungamornrat, J., Rajapakse, R.K.N.D.: Surface elasticity and residual stress effect on the elastic field of a nanoscale elastic layer. Interact. Multiscale Mech. **4**, 85–105 (2011)

Jing, G.Y., Duan, H.L., Sun, X.M., Zhang, Z.S., Xu, J., Li, Y.D., et al.: Surface effects on elastic properties of silver

nanowires: contact atomic-force microscopy. Phys. Rev. B **73**, 235409 (2006)
Koguchi, H.: Surface Green function with surface stresses and surface elasticity using Stroh's formalism. J. Appl. Mech. **75**, 061014 (2008)
Lai, J., Bakker, A.: 3-D Schapery representation for nonlinear viscoelasticity and finite element implementation. Comput. Mech. **18**, 182–191 (1996)
Liu, C., Rajapakse, R.K.N.D., Phani, A.S.: Finite element modeling of beams with surface energy effects. J. Appl. Mech. **78**, 031014 (2011)
Long, J.M., Wang, G.F.: Effects of surface tension on axisymmetric Hertzian contact problem. Mech. Mater. **56**, 65–70 (2013)
Long, J.M., Wang, G.F., Feng, X.Q., Yu, S.W.: Two dimensional Hertzian contact problem with surface tension. Int. J. Solids Struct. **49**, 1588–1594 (2012)
Lu, P., He, L.H., Lee, H.P., Lu, C.: Thin plate theory including surface effects. Int. J. Solids Struct. **43**, 4631–4647 (2006)
Mahmoud, F.F., El-Shafei, A.G., Abdelrahman, A.A., Attia, M.A.: Modeling of nonlinear viscoelastic contact problems with large deformations. Appl. Math. Model. **37**, 6730–6745 (2013)
Miller, R.E., Shenoy, V.B.: Size dependent elastic properties of nanosized structural elements. Nanotechnology **11**(3), 139–147 (2000)
Mogilevskaya, S.G., Crouch, S.L., Stolarski, H.K.: Multiple interacting circular nano-inhomogeneities with surface/interface effects. J. Mech. Phys. Solids **56**(6), 2298–2327 (2008)
Nix, W.D., Gao, H.: Indentation size effects in crystalline materials: a law for strain gradient plasticity. J. Mech. Phys. Solids **46**, 411–425 (1998)
Pinyochotiwong, Y., Rungamornrat, J., Senjuntichai, T.: Rigid frictionless indentation on elastic half space with influence of surface stresses. Int. J. Eng. Sci. **71**, 15–35 (2013)
Ru, C.Q.: Simple geometrical explanation of Gurtin–Murdoch model of surface elasticity with clarification of its related versions. J. Phys. Mech. Astron. **53**, 536–544 (2010)
Schapery, R.A.: On the characterization of nonlinear viscoelastic materials. Polym. Eng. Sci. **9**(4), 295–310 (1969)
Schapery, R.A.: Correspondence principles and a generalized J integral for large deformation and fracture analysis of viscoelastic media. Int. J. Fract. **25**, 195–223 (1984)
Shaat, M., Eltaher, M.A., Gad, A.I., Mahmoud, F.F.: Nonlinear size dependent finite element analysis of functionally graded tiny bodies. Int. J. Mech. Sci. **77**, 356–364 (2013a)
Shaat, M., Mahmoud, F.F., Alieldin, Alshorbagy, A.E.: Finite element analysis of graded nanoscale films. Finite Elem. Anal. Des. **74**, 41–52 (2013b)
Sharma, P., Wheeler, L.T.: Size dependent elastic state of ellipsoidal nano-inclusions incorporating surface/interface tension. J. Appl. Mech. **74**, 447–454 (2007)
Sharma, P., Ganti, S., Bhate, N.: Effect of surfaces on the size dependent elastic state of nano-inhomogeneities. Appl. Phys. Lett. **82**, 535–537 (2003)
Shenoy, V.B.: Atomistic calculations of elastic properties of metallic FCC crystal surfaces. Phys. Rev. B **71**, 094104 (2005)
Tang, G., Shen, Y.L., Singh, D.R.P., Chawla, N.: Analysis of indentation-derived effective elastic modulus of metal-ceramic multilayers. Int. J. Mech. Mater. Des. **4**(4), 391–398 (2008)
Tian, L., Rajapakse, R.K.N.D.: Elastic field of an isotropic matrix with a nanoscale elliptical inhomogeneity. Int. J. Solids Struct. **44**, 7988–8005 (2007)
Wang, G.F., Feng, X.Q.: Effects of surface stresses on contact problems at nanoscale. J. Appl. Phys. **101**, 013510 (2007)
Wang, G., Bian, J., Feng, J., Feng, X.: Compressive behavior of crystalline nanoparticles with atomic-scale surface steps. Mater. Res. Express **2**(1), 015006 (2015)
Wang, Z.Q., Zhao, Y.P., Huang, Z.P.: The effects of surface tension on the elastic properties of nano structures. Int. J. Eng. Sci. **48**(2), 140–150 (2010)
Wriggers, P.: Computational Contact Mechanics, 2nd edn. Springer, Berlin (2006)
Yakobson, B.I.: Nanomechanics. In: Goddard, W.A., Brenner, D.W., Lyshevski, S.E., Iafrate, G.J. (eds.) Handbook of Nanoscience, Engineering and Technology, pp. 17.1–17.18. CRC Press, Florida (2003)
Zhao, X.J., Rajapakse, R.K.N.D.: Analytical solutions for a surface-loaded isotropic elastic layer with surface energy effects. Int. J. Eng. Sci. **47**, 1433–1444 (2009)
Zhao, X.J., Rajapakse, R.K.N.D.: Elastic field of a nano-film subjected to tangential surface load: asymmetric problem. Eur. J. Mech. A Solids. **39**, 69–75 (2013)
Zhao, X. J.: Surface loading and Rigid Indentation of an Elastic Layer with Surface Energy Effects. Master thesis, The University of British Columbia, Vancouver, Canada (2009)
Zhou, S., Gao, X.L.: Solutions of half-space and half-plane contact problems based on surface elasticity. ZAMP **64**, 145–166 (2013)
Zhou, S.: New Solution of Half Space Contact Problems Using Potential Theory, Surface Elasticity and Strain Gradient Elasticity, PhD dissertation, Texas A&M University (2011)
Zocher, M.A., Groves, S.E., Allen, D.H.: A three dimensional finite element formulation for thermoviscoelastic orthotropic media. Int. J. Numer. Methods Eng. **40**, 2267–2280 (1997)